AD-A117 425 NATIONAL AERONUATICS AND SPACE ADMINISTRATION MOFFET--ETC F/G 20/4
HOLOGRAPHIC INTERFEROMETRY TECHNIQUE FOR ROTARY WING AERODYNAMI--ETC(U)
JUN 82 J K KITTLESON, Y H YU

UNCLASSIFIED

NL

1 of 1

END
DATE
FILMED
8 82
DTIC

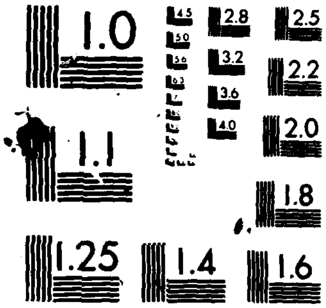
1.0
4.5
5.0
5.6
6.3
2.8
3.2
3.6
4.0
2.5
2.2
2.0
1.1
1.8
1.25
1.4
1.6

(1) 18 JUN 1982

# HOLOGRAPHIC INTERFEROMETRY TECHNIQUE FOR ROTARY WING AERODYNAMICS AND NOISE (U)

*JOHN K. KITTLESON
YUNG H. YU, DR.
AEROMECHANICS LABORATORY (AVRADCOM)
AMES RESEARCH CENTER, NASA
MOFFETT FIELD, CALIFORNIA 94035

## INTRODUCTION

Helicopter impulsive noise, sometimes called "blade slap," is the most annoying and easily detectable sound generated by a helicopter. This extremely loud noise is generated by two different mechanisms which occur on the main and tail rotors of modern helicopters. One phenomenon, labeled high-speed impulsive noise, occurs on the advancing-blade side of the rotor disc where advancing blade Mach numbers are quite high ($M_T \approx 0.90$) and local transonic flow is inevitable. Rotor-blade thickness near the tip causes a low-frequency "thumping" and results in a nearly symmetrical acoustic signature (Figs. 1a and 1b). As the Mach number increases, local transonic events distort and amplify the time history waveform (Fig. 1c). The resulting sawtooth waveform, which radiates large amounts of acoustic energy, causes the sound to be very intense and distinctive.

The second phenomenon responsible for impulsive noise is known to occur when the rotor blades interact with previously generated tip vortices ~~(1)~~. Much less is known about the essential mechanisms in this case. Mach number and wake geometry are thought to play key roles in the ultimate strength of the resulting blade-vortex interaction noise. This sound is known to be a significant problem during descent and deceleration and can occur on both the advancing and retreating sides of the helicopter disc. However, it is believed that the advancing-blade interactions radiate significantly more energy.

Both of the mechanisms for loud impulsive noise have one parameter in common - high Mach number flow. For high-speed impulsive noise, local shocks on the blade surface have been shown to extend off the tip of the blade directly to the acoustic far field (Fig. 2). These shocks directly affect the amount of energy that is radiated by the helicopter. Detailed predictions of the far-field acoustics depend critically on the physical phenomena in the tip region. In particular, the three-dimensional velocity

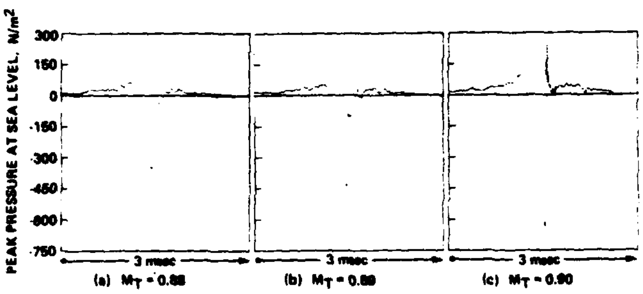

Figure 1. Waveform transition; the development of a radiating discontinuity, in-plane, r/D = 1.5 (from Ref. 2).

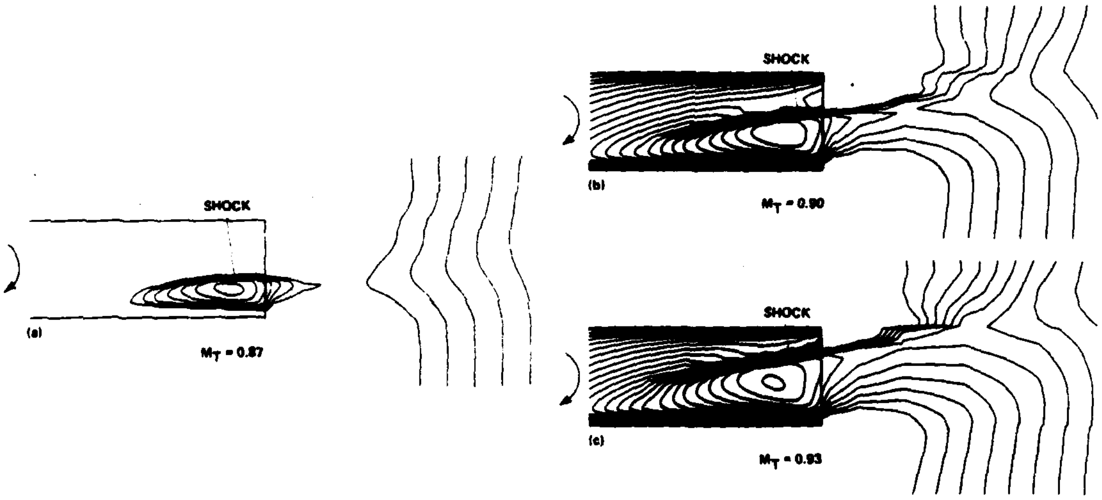

Figure 2. Velocity contours near a rotor tip in the transonic range (from Ref. 9).

distribution over a volume large enough to capture the local shock waves is required (2). The blade-vortex interaction problem also requires a vast quantity of local transonic flow information. In particular, unsteady local shocks and their resulting pressure *distribution* near the blade surface, as well as flow characteristics (e.g., vortex geometry and inflow), are required. In both cases, good experimental data of the three-dimensional transonic flow field around a rotor blade and its wake system are essential for the theoretical prediction of the acoustic signature. The measurements are also required for the verification of aerodynamic transonic flow numerical codes.

Unfortunately, conventional visualizing and measuring techniques have severe limitations when applied to the large three-dimensional transonic flow field near a rotor. Hot-wire anemometry disturbs the flow and measures only one point at a time. Laser velocimetry requires seeding of the flow (which can be inaccurate because of acceleration effects) and also measures only one point at a time. Classical interferometry (such as Mach-Zehnder) divides the interfering waves spatially, requiring very expensive optical components and making large-scale experiments almost impossible. Schlieren and shadowgraph photography provide only a two-dimensional representation of a three-dimensional flow field. Clearly, another technique which overcomes these limitations must be employed.

Recent developments in the field of holographic interferometry in combination with computerized tomography proves to be the most promising technique for both visualizing and quantitatively measuring the flow field near a rotor blade. Holographic interferometry is nonintrusive and can be applied to a large-scale experiment with relatively low cost. It also records information over a large volume on a single interferogram, and can be used to visualize the flow field in a three-dimensional manner. To date, most applications of this technique have been limited to two-dimensional flow (3), axis-symmetric flow, or a simple three-dimensional flow with a small model under ideal laboratory conditions (4,5).

In this paper, the concepts of holography and holographic interferometry, as applied to the visualization and measurement of the three-dimensional flow field near a rotor tip, are previewed, and initial experimental results of investigations of local shock structures and tip vortices behind the blade are presented. An additional method to visualize the flow in a three-dimensional manner is demonstrated, and finally, a method to quantitatively measure the three-dimensional flow, which will provide the necessary information to help improve helicopter performance and reduce noise, is introduced.

## BACKGROUND CONCEPTS

### Holography

Holography is a two-step imaging process which records and reconstructs diffracted light waves (6,7). An interference pattern is formed on film by adding a coherent reference wave to the object wave (the wave of interest), as shown in Fig. 3a. The irradiance at the film plane is

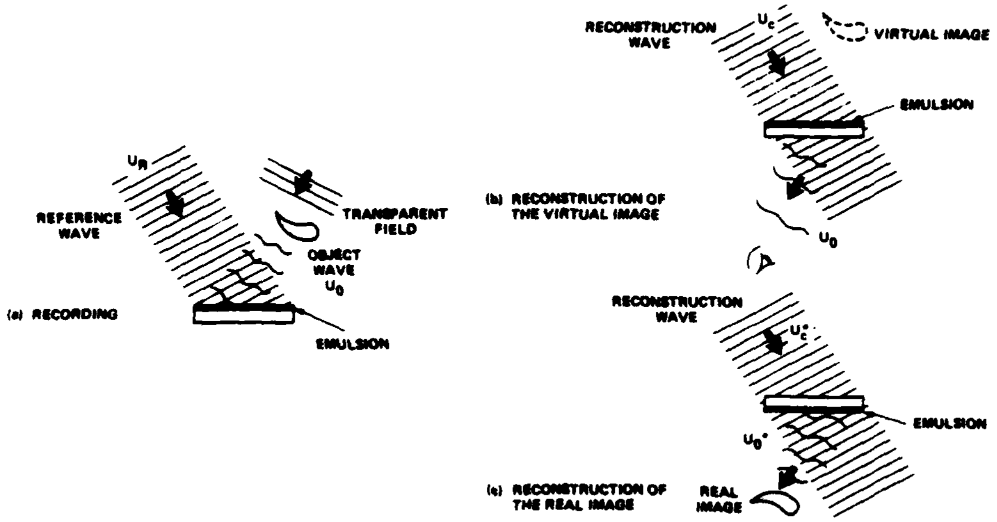

Figure 3. Optical holography recording and reconstruction.

$$\begin{aligned} I &= |U_R + U_o|^2 \\ &= I_R + I_o + U_R^*U_o + U_RU_o^* \end{aligned} \tag{1}$$

where $U_R$ represents the reference wave, $U_o$ represents the object wave, $I_R$ and $I_o$ are amplitude squares of the reference and object waves, and the asterisk represents a conjugate wave. The last two terms in Eq. (1) represent the interference pattern recorded on the film, which contains both amplitude and phase information.

The amplitude transmittance of the developed film, called a hologram, is proportional to the irradiance

$$t = \beta(I_R + I_o) + \beta U_R^*U_o + \beta U_RU_o^*$$

where $\beta$ is a property of the film. When the reconstruction wave $U_c$ illuminates the hologram as shown in Fig. 3b, the transmitted light is

$$U_I = U_ct = \beta U_c(I_R + I_o) + \beta U_R^*U_cU_o + \beta U_RU_cU_o^* \tag{2}$$

The first term of Eq. (2) represents an undiffracted zero-order wave. The second and third terms represent two first-order diffracted waves. The second and most important term of Eq. (2) can be written as $(\beta U_R^*U_c)U_o$. This is a replica of the original object wave $U_o$.

If the hologram is rotated 180° about a vertical axis so that the emulsion of the hologram is placed on the observer's side, the transmitted light with the reconstruction wave $U_c{}^*$ will be

$$U_I = U_c{}^*t = \beta U_c{}^*(I_R + I_o) + \beta U_R{}^*U_c{}^*U_o + \beta U_R U_c{}^*U_o{}^* \qquad (3)$$

The last term of Eq. (3) can be written as $(\beta U_R U_c{}^*)U_o{}^*$; it represents a reconstructed wave that is conjugate to the original object wave. A real image in space is formed on the observer's side of the hologram, as shown in Fig. 3c. The real image can be photographed without the use of a lens by placing a sheet of photographic film in the real-image space.

## Holographic Interferometry

Holographic interferometry is the interferometric comparison of two object waves that are recorded holographically. Although holographic interferograms and classical Mach-Zehnder interferograms are similar in many respects, there are some advantages in using holographic interferograms for this project.

Holographic interferometry has the very important property of cancellation of pathlength errors. In a classical interferometer, the interfering light waves are divided spatially. That is, the two interfering waves are recorded simultaneously but travel different paths. Any difference in pathlengths in the optical system would give rise to extraneous fringes, which could be eliminated only by using very high quality optics. This is a difficult and expensive requirement to meet when using large optical components such as were used in this experiment. However, in a holographic interferometer, the two interfering object waves are divided temporally. That is, the two interfering waves are recorded at two different times but travel the same path. Since there is no difference in the pathlength of the two interfering object waves in the optical system, only changes in the pathlength between exposures in the flow field are displayed. This makes it possible to use relatively low quality 2-ft-diameter mirrors in the optical system.

A double-exposure holographic interferogram is made by holographically recording two object waves sequentially in time. The first exposure records the undisturbed object wave (Fig. 4a), and the second exposure records the disturbed object wave (Fig. 4b). The irradiance at the film plane is

$$\begin{aligned} I &= |U_R + U_{o1}|^2 + |U_R + U_{o2}|^2 \\ &= 2I_R + I_{o1} + I_{o2} + U_R{}^*(U_{o1} + U_{o2}) + U_R(U_{o1} + U_{o2})^* \qquad (4) \end{aligned}$$

where $U_{o1}$ represents the undisturbed object wave, and $U_{o2}$ represents the disturbed object wave. As in single-exposure holography, the last two

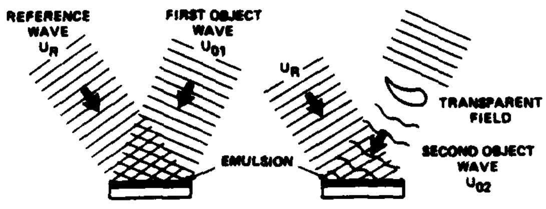

(a) FIRST-EXPOSURE RECORDING (b) SECOND-EXPOSURE RECORDING

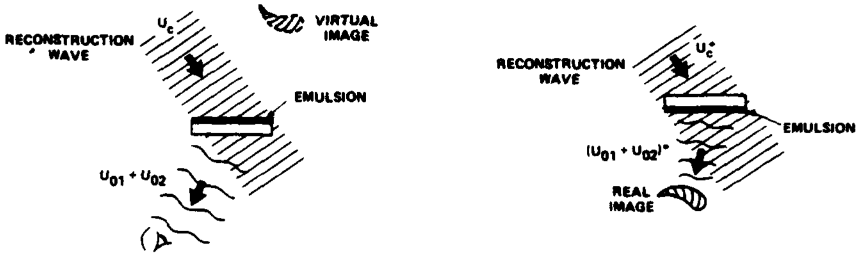

(c) RECONSTRUCTION OF THE VIRTUAL IMAGE (d) RECONSTRUCTION OF THE REAL IMAGE

Figure 4. Double-exposure holographic interferometry.

terms of Eq. (4) represent the interference pattern recorded on the film, which contains both amplitude and phase information.

The amplitude transmittance of the developed film, called a holographic interferogram, is proportional to the irradiance

$$t = \beta(2I_R + I_{o1} + I_{o2}) + \beta U_R^*(U_{o1} + U_{o2}) + \beta U_R(U_{o1} + U_{o2})^*$$

When the reconstruction wave $U_c$ illuminates the interferogram as shown in Fig. 4c, the transmitted light is

$$U_I = U_c t = \beta U_c(2I_R + I_{o1} + I_{o2}) + \beta U_R^* U_c(U_{o1} + U_{o2}) + \beta U_R U_c(U_{o1} + U_{o2})^* \quad (5)$$

The second term of Eq. (5), $\beta U_R^* U_c(U_{o1} + U_{o2})$, is the composite virtual image reconstruction of the two object waves $(U_{o1} + U_{o2})$. The composite real-image reconstruction can be obtained by rotating the interferogram 180° about the vertical axis (Fig. 4d).

Recall that the irradiance of the reconstructed wave is proportional to

$$I = |U_{o1} + U_{o2}|^2$$

which can be written as (6,7)

$$I = 2A^2[1 + \cos(\Delta\phi)] \tag{6}$$

where A is the amplitude of the object waves, and $\Delta\phi$ is the optical pathlength difference between the two object waves. Equation (6) represents an interferogram with a fringe pattern $2[1 + \cos(\Delta\phi)]$. Dark and bright fringes are contours of constant values of $\Delta\phi$, where $\Delta\phi$ is given by

$$\Delta\phi = \int_s k(\rho - \rho_0)ds = N\lambda \tag{7}$$

and where k is the Gladstone-Dale constant, which is a property of the gas ($k = 0.225\ m^3/kg$ for air); $\rho$ and $\rho_0$ are density values for the disturbed and undisturbed air; N is the fringe order number; and $\lambda$ is the wavelength of the ruby laser ($\lambda = 0.6943\ \mu m$). Equation (7) shows that the fringe patterns are the integrated values of local density differences $(\rho - \rho_0)$ along the path length s. An interferogram is thus a two-dimensional projection of a three-dimensional field. For an asymmetric three-dimensional flow field, several interferograms at various azimuthal angles must be analyzed to invert the integral to obtain the density value at a specific point.

## EXPERIMENTAL SETUP AT THE ANECHOIC HOVER CHAMBER

The basic optical system required to record interferograms of the flow field around a rotor tip is shown in Fig. 5. The actual test setup in the Anechoic Hover Chamber at the Aeromechanics Laboratory is shown in Fig. 6. A pulsed ruby laser, with a very short pulse width, is used to "freeze" the rotor at any desired azimuthal angle. The object wave is expanded by a beam expander and collimated by a large spherical mirror to a 2-ft-diameter beam as it passes through the region of interest. The reference wave is lengthened (the difference in path lengths of the object wave and the reference wave must remain within the 7-ft coherence length of the ruby laser), expanded, and collimated. The two waves are brought together at the photographic film plate.

The first exposure is recorded by exposing the film plate while the blade is stationary. Ideally, the air in this case has no velocity and a uniform density distribution. The second exposure is recorded by exposing the same film plate while the blade is rotating. The nonhomogeneous density distribution introduces phase changes in the second object wave which give rise to an interference pattern on the film plate. The photographic plate is then removed from the Hover Chamber, developed, and reconstructed in a convenient place with a continuous-wave He-Ne laser.

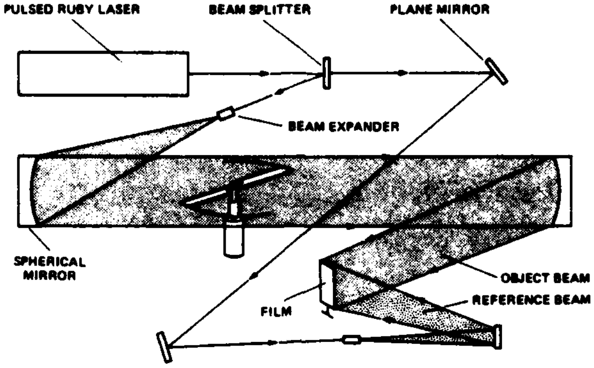

Figure 5. Basic holographic interferometry system.

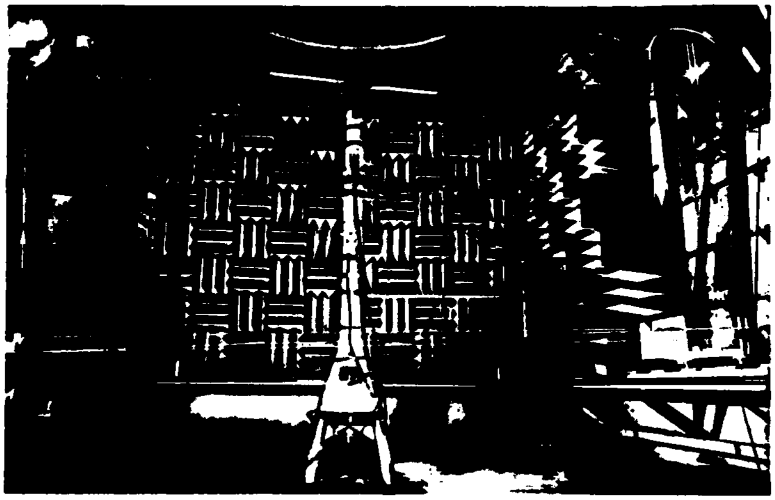

Figure 6. Actual holographic interferometry setup at the Anechoic Hover Chamber.

## EXPERIMENTAL RESULTS

### Effect of Tip Mach Number

Shock formation and its connection to the far field is very important in understanding the acoustic waveform transition, as shown in Fig. 1. The progress of shock formation can be seen in double exposure interferograms at various tip Mach numbers (Fig. 7). For $M_T = 0.88$ there is very little

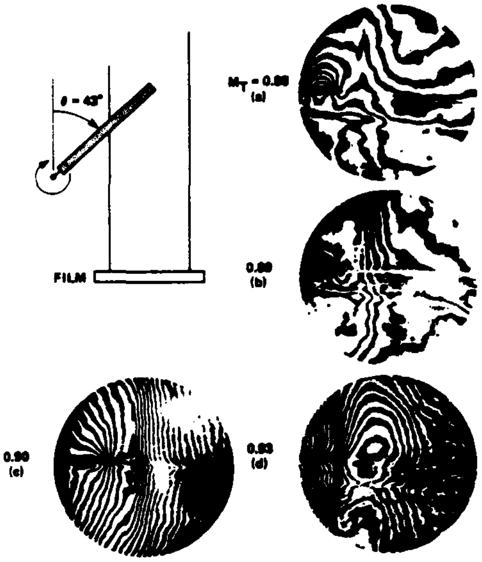

Figure 7. Interferograms at various tip Mach numbers.

shock extension beyond the blade tip (Fig. 7a). For $M_T$ = 0.89 the shock is about to extend to the far field (Fig. 7b). For these conditions the local shock is confined to the neighborhood of the blade (Fig. 2a), while the far-field acoustic waveform generally maintains a symmetric shape (Figs. 1a and 1b). However, for $M_T$ = 0.90 the shock has extended to the far field (Figs. 7c and 2b). The characteristics of the shock structure can now propagate to the far field, generating an abrupt change in the acoustic waveform. A discontinuity on the compression side of a sawtooth waveform results (Fig. 1c). This discontinuity produces extremely annoying high-frequency components of sound. For $M_T$ = 0.93 the shock has strengthened in intensity and moved to near the trailing edge of the rotor (Figs. 7d and 2c). The acoustic waveform widens while maintaining a discontinuity on the compression side. Note that the shock appears to move inboard for increasing tip Mach numbers in Fig. 7. This is because the shock bends farther backward for higher tip speeds (Figs. 2b and 2c).

## Interferograms at Various Azimuthal Angles

As previously mentioned, to determine the density value at a specific point in the flow field, Eq. (7) must be inverted. This inversion can be performed only if several interferograms at various azimuthal angles around the flow field are analyzed. Information from these interferograms will be combined with a computer tomography algorithm to determine the density value at any point of interest in the flow field. Figure 8 shows several

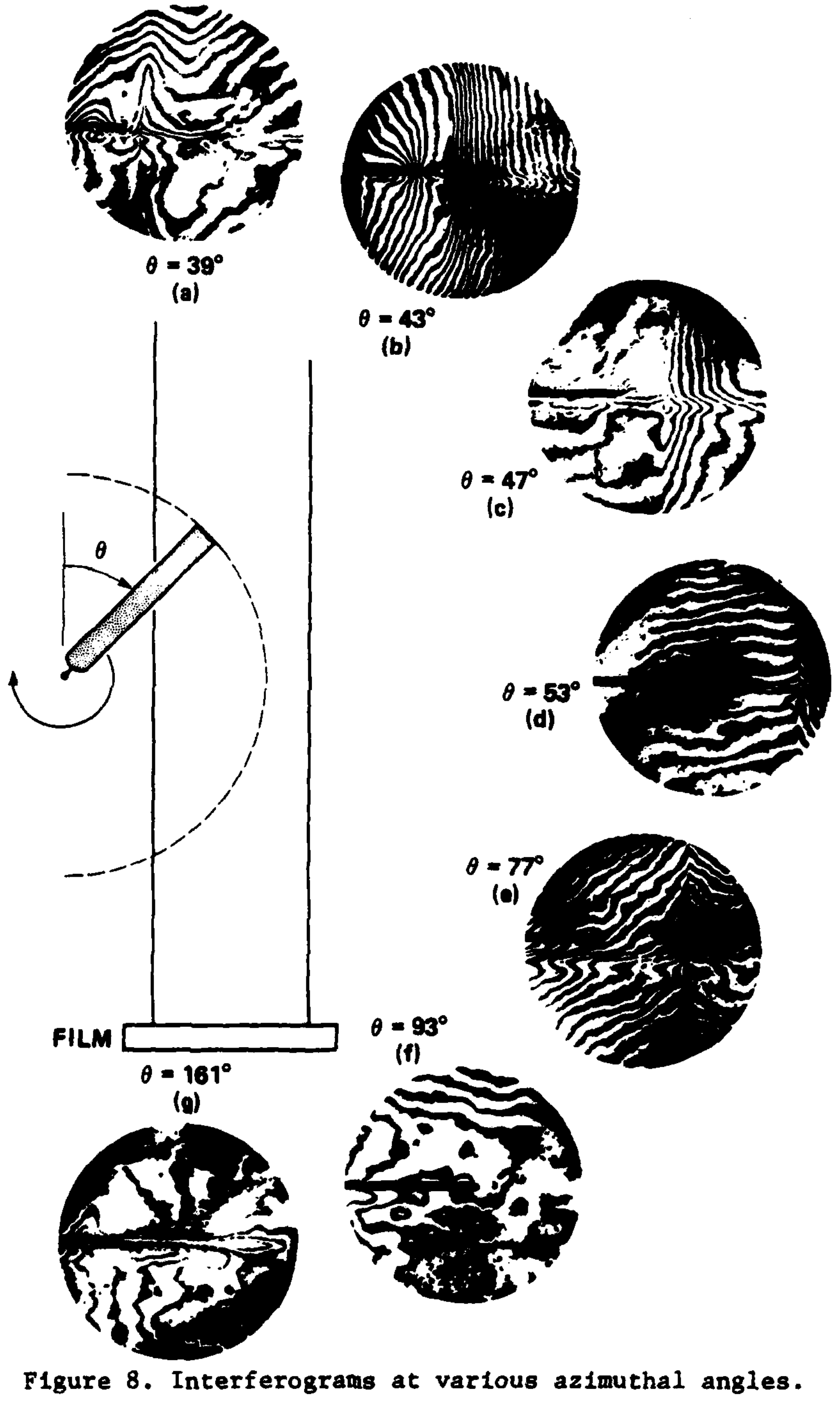

Figure 8. Interferograms at various azimuthal angles.

interferograms at various azimuthal angles for a rotor with $M_T = 0.90$. The shock extension to the far field can be seen in Figs. 8a-8e but not in Figs. 8f and 8g. This is basically a result of part of the shock being parallel to the optical path (creating a large phase change) in Figs. 8a-8e, while the shock is generally perpendicular to the optical path (creating very little phase change) in Figs. 8f and 8g.

## Wake System and Tip-Vortex Trajectory

The tip-vortex geometrical position and strength play the dominant role in studies of blade-vortex interactions. This interaction generates unsteady pressure fluctuations over the blade, contributing to the impulsive nature of the acoustic wave and to the severe vibration felt by helicopter passengers. Figure 9 shows the details of tip vortices generated by two rotor blades. This is an interferogram where $M_T = 0.4$ and the collective pitch angle is 8°. The downwash and contraction of the tip vortices obtained from this interferogram agree reasonably well with hot-wire measurements (8) (Fig. 10).

## Three-Dimensional Visualization

Holographic interferometry provides the unique ability to visualize a three-dimensional field with a single interferogram. Although no quantitative information will be obtained, this visualization can aid in understanding the geometry of a field. To illustrate this point, a simple test was carried out as shown in Fig. 11. The model consists of three objects: (1) a double post near the film plate, (2) a heating element and model rotor blade slightly farther from the film plate, and (3) a single post farther still from the film plate. A diffuser was inserted into the object wave and a double-exposure interferogram was recorded. The first exposure was made with the heating element at room temperature, simulating a stationary blade. The second exposure was made with the heating element at a

Figure 9. Double-exposure interferogram of tip vortices at $M_T = 0.4$ and collective pitch angle of 8° (NACA 0012, aspect ratio = 13.7).

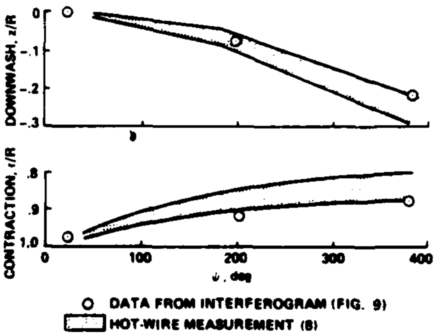

Figure 10. Comparison of hot-wire and holographic interferometry measurement of tip vortices position.

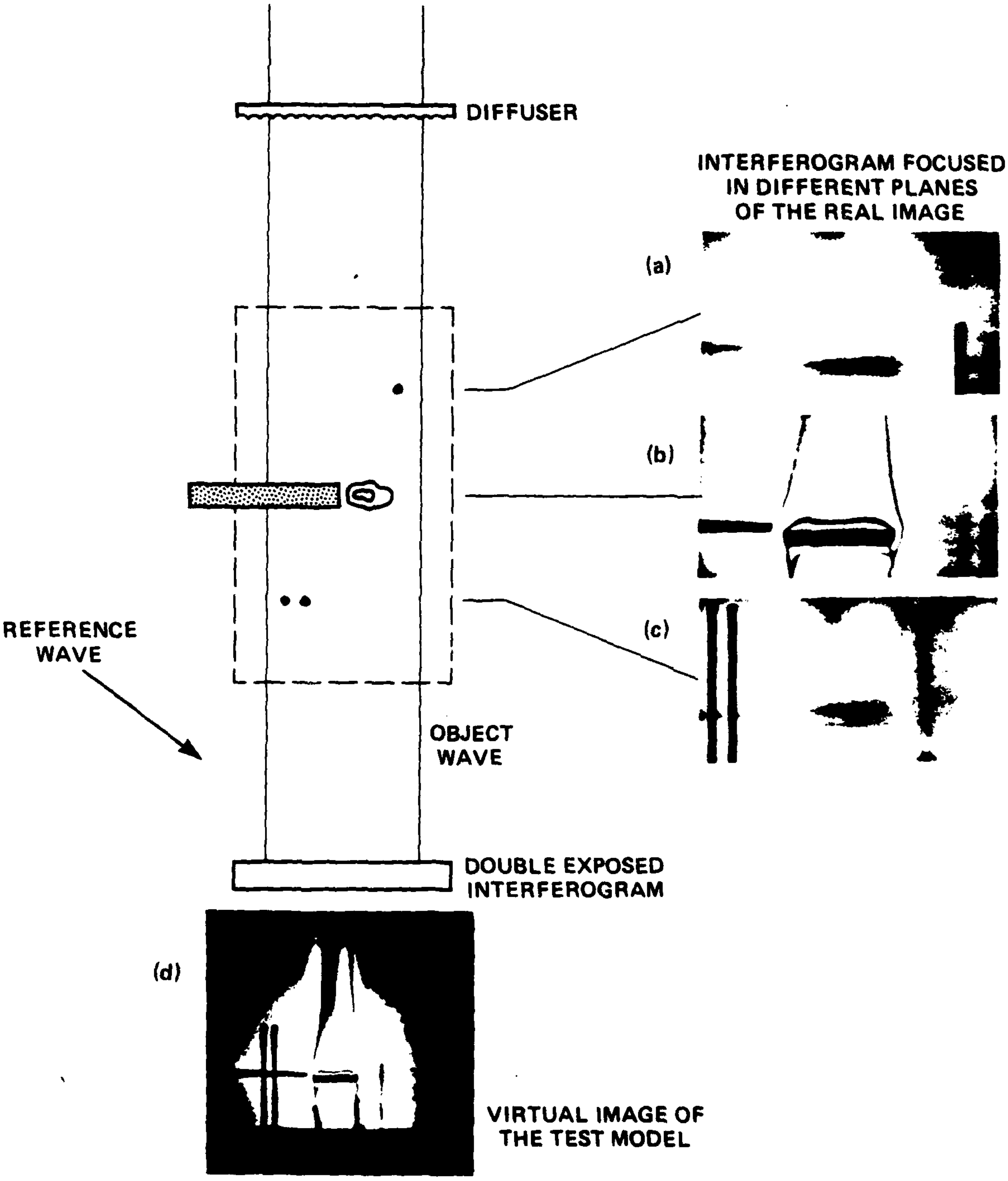

Figure 11. Three-dimensional visualization.

high temperature, creating a nonhomogeneous density distribution in the air and thus simulating a rotating blade. The three-dimensional virtual image was reconstructed and photographed (Fig. 11d). The real image was reconstructed and photographed at three planes in the real-image space (Figs. 11a-11c). It is possible to determine the distribution of density change by noting where the fringes come into focus.

## CONCLUDING REMARKS

A holographic interferometry technique has been demonstrated as the most promising method for both visualizing and quantitatively measuring the three-dimensional transonic flow field near a rotor blade. This technique overcomes many limitations of conventional experimental techniques and has yielded some initial results.

Holographic interferograms show the behavior of shock structures near a high-speed rotor tip. Interferograms recorded at various tip Mach numbers ($M_T$ = 0.88 to 0.93) verify the formation of a local shock and its extension to the far field at high tip Mach numbers. Interferograms recorded at various azimuthal angles show the general position and shape of an extended shock structure. The position and shape of such a shock recorded in these interferograms is in general agreement with numerical calculations.

Holographic interferograms also show the geometrical position of tip vortices behind a rotor blade. The characteristic rotor contracted slip stream is clearly visible. The contraction and downwash position of the tip vortices recorded in this interferogram agrees reasonably well with hot-wire anemometry measurements.

In the future, an additional method to visualize the flow in a three-dimensional manner will be employed. Double-exposure holographic interferograms will be recorded with a diffuser added to the optical system. The reconstructed real image can be photographed in any desired plane to identify the position of the shock.

To quantitatively measure the three-dimensional flow field near a high-speed rotor, several interferograms must be analyzed. This is because an interferogram records integrated information and is therefore a two-dimensional projection of the three-dimensional flow field. Interferograms recorded of various azimuthal angles will be processed with a computer tomography algorithm to determine the velocity at a specific point. This experimental quantitative measurement of the three-dimensional transonic velocity field near a rotor blade, with detailed information of the shock structure and wake system, will help the researcher of both acoustics and aerodynamics to design a better blade at high tip speeds.

## ACKNOWLEDGMENTS

We thank several of our colleagues at the Aeromechanics Laboratory for their unselfish contributions to this effort, especially Mr. H. Andrew Morse and Dr. Fredric Schmitz for their consistent and untiring support. We also owe a special thanks to Professor Charles Vest of the University of Michigan for many fruitful discussions and guidance.

## REFERENCES

1. Boxwell, D.A.; and Schmitz, F. H.: Full-Scale Measurements of Blade-Vortex Interaction Noise. Presented at the 36th Annual Forum of the American Helicopter Society, paper No. 61, May 1980.

2. Schmitz, F. H.; and Yu, Y. H.: Transonic Rotor Noise - Theoretical and Experimental Comparisons. Vertica, vol. 5, 1981, pp. 55-74.

3. Johnson, D. A.; and Bachelo, W. D.: Transonic Flow about a Two-Dimensional Airfoil - Inviscid and Turbulent Flow Properties. AIAA Paper 78-1117, July 1978.

4. Matulka, R. D.; and Collins, D. J.: Determination of Three-Dimensional Density Fields from Holographic Interferometry. J. Appl. Phys., vol. 42, 1971, pp. 1109-1119.

5. Sweeney, D. W.; and Vest, C. M.: Reconstruction of Three-Dimensional Refractive Index Field from Multidirectional Interferometric Data. Appl. Opt., vol. 12, 1973, pp. 2649-2664.

6. Vest, C. M.: Holographic Interferometry. Wiley-Interscience, 1979.

7. Collier, R. J.; Burckhardt, C. B.; and Lin, L. H.: Optical Holography. Academic Press, 1971.

8. Tung, C.; Pucci, S. L.; Caradonna, F. X.; and Morse, H. A.: The Structure of Trailing Vortices Generated by Model Rotor Blades. NASA TM-81316, 1981.

9. Caradonna, F. X.: The Transonic Flow on a Helicopter Rotor. Ph.D. Dissertation, Stanford U., Stanford, Calif., Mar. 1978.

END

DATE
FILMED

8 82

DTIC